GEOPHYSICS, VOL. 66, NO. 5 (SEPTEMBER-OCTOBER 2001); P. 1340–1348, 14 FIGS.

Case History

Integrated wide-angle and near-vertical subbasalt study using large-aperture seismic data from the Faeroe–Shetland region

Juergen Fruehn*, Moritz M. Fliedner‡, and Robert S. White‡

ABSTRACT

Acquiring large-aperture seismic data (38 km maximum offset) along a profile crossing the Faeroe–Shetland basin in the North Atlantic enables us to use wide-angle reflections and refractions, in addition to conventional streamer data (0–6 km), for subbasalt imaging. The wide-angle results are complemented and confirmed by images obtained from the conventional near-vertical-offset range. Traveltime tomography applied to the wide-angle data shows a low-velocity layer (3.5–4.5 km/s) underneath southeastward-thinning lava flows, suggesting a 2.5–3.0-km-thick sedimentary layer. The velocity model obtained from traveltime tomography is used to migrate wide-angle reflections from large offsets that arrive ahead of the water-wave cone. The migrated image shows base-basalt and sub–basalt reflections that are locally coincident with the tomographic boundaries. Application of a new multiple suppression technique and controlled stacking of the conventional streamer data produces seismic sections consistent with the wide-angle results. Prestack depth migration of the near-vertical offsets shows a continuous base-basalt reflection and a clearly defined termination of the basalt flows.

INTRODUCTION

The Faeroe–Shetland region (Figure 1) has been subject recently to intense exploration activity, the main objective being to image the structure of potentially hydrocarbon-bearing sediments buried beneath early Tertiary basalt flows extending from the Faeroe Islands. These sediments accumulated in rift-related basins from Triassic to earliest Tertiary times (Stoker et al., 1993). With continental stretching and eventual breakup, huge volumes of basalt were produced by decompression melting of the Icelandic mantle plume (White and McKenzie, 1989; Eldholm and Grue, 1994; Barton and White, 1997a,b). In the Faeroes region, the main locus of rifting and the bulk of the fissures from which basalt was extruded probably lay west of the present Faeroe Islands in the region of the continent–ocean boundary (Richardson et al., 1998). From these fissures, basalt flowed eastward across the sediments in the Faeroe–Shetland basin, mostly near or just above sea level at the time (Waagstein, 1983).

This region presents considerable challenges for seismic imaging. The thick, inhomogeneous basalt creates a barrier to imaging the underlying structure using conventional seismic data. Synthetic seismogram modeling shows that reflected subbasalt energy in this offset range is up to a hundred times lower than energy reflected from the basalt and sedimentary overburden (unpublished data from this study). Multiple arrivals from the highly reflective top of the basalt and the overburden reflectors are therefore likely to obscure subbasalt primary reflections. Multiple suppression techniques based on the periodicity of the multiples, rather than on their move-out, are helpful in these circumstances. However, the amplitude of residual multiples and/or the degree to which primaries are affected by the procedure often yields an equivocal subbasalt image that cannot be interpreted on its own. Correlation with wide-angle seismic images is therefore crucial for interpretation.

The acquisition of large-aperture seismic data allows application of a variety of analysis and imaging techniques that help overcome some of the problems faced by conventional seismic reflection profiling. Since reflection amplitudes generally increase with offset, subbasalt reflections are more easily identifiable at wide than at near angles. Wide-angle arrivals are also less affected by multiples from the overburden as a consequence of the increasing difference in traveltime and move-out

Manuscript received by the Editor December 29, 1999; revised manuscript received October 13, 2000.
*Formerly Bullard Laboratories, University of Cambridge, Cambridge, U.K. Presently GX Technology, Lawrence House, 45 High St., Egham TW20 9DP, U.K. E-mail: jkf@gxt.com.
‡Bullard Laboratories, University of Cambridge, Madingley Road, Cambridge CB3 0EZ, U.K. E-mail: moritz@esc.cam.ac.uk; rwhite@esc.cam.ac.uk.

between the different phases. Migration or stacking of wide-angle reflections is thus more likely to yield an interpretable seismic section of subbasalt arrivals than is use of the near-vertical offset range alone. The large aperture also enables refracted arrivals, which are usually muted out in conventional seismic processing, to be recorded. They carry considerable information on the velocity structure—particularly of the basalt and the basement—and are crucial for traveltime tomography. Wide-angle reflections and refractions are both used to build a well-constrained tomographic image of the crustal structure.

Data acquisition was undertaken in summer 1996 by Western Geophysical and the Amerada Hess Partner Group [Amerada Hess, LASMO (ULX), Norsk Hydro and DOPAS]. A two-ship geometry and subsequent processing yielded shot gathers that we call supergathers, with an offset range of 0.2 to 38.2 km (e.g., Figure 2). A detailed description of the two-ship technique and acquisition parameters is given in White et al. (1999).

METHOD

A variety of techniques was applied to this data set to obtain an internally consistent and well-constrained image of the structure along profile FLARE 96-1 (Figure 1).

A key to traveltime tomography is identifying the useful arrivals. In this data set, they are those refracted through the basalt, reflected off its base, and returned from below the basalt. Identification is aided by synthetic seismogram modeling of test models.

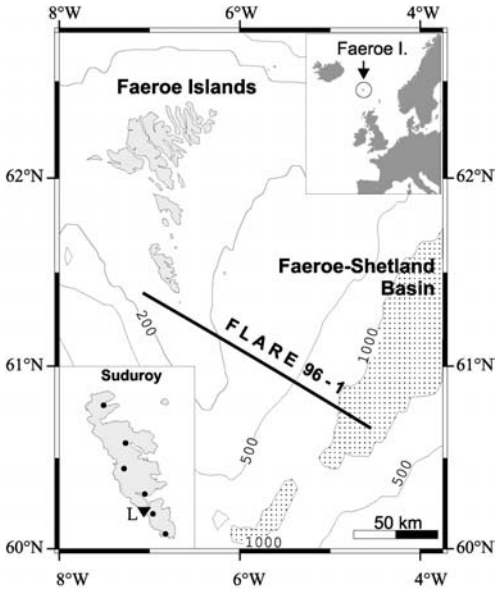

FIG. 1. Location of FLARE 96-1 profile. Upper inset—location of Faeroe Islands within the North Atlantic. Lower inset—positions of land seismometers on Suduroy used to record offshore airgun shots. Triangle *L* is the location of the Lopra borehole. Water-depth contours are in meters; depths >1000 m are stippled.

The traveltimes of the wide-angle arrivals from a subset of the supergathers are used in a 2-D tomographic inversion to derive a velocity model. This model already represents a valuable end result in its own right but is also a prerequisite for prestack depth migration.

A series of constant-velocity stacks is performed in parallel as a rapid way to confirm the existence of primary subbasalt events at wide angles. At this stage of the study, a laterally variable velocity model and seismic images of the main subbasalt boundaries have resolved the low-resolution structure of the subsurface.

The near-vertical data set adds high-resolution detail to the wide-angle image after applying a new multiple suppression technique. Subsequent semblance analysis and controlled stacking (to boost the contribution of subbasalt reflections against that of residual multiples) reveals the base-basalt reflector or, in cases where the basalt is thin, some deeper subbasalt reflections.

Kirchhoff prestack depth migration is performed using a combination of velocities derived from semblance analysis (shallow structure) and traveltime tomography (deep structure). By merging migrations from different offset ranges (near vertical for the sediment section above the basalt and wide angle for the intrabasalt and subbasalt sections), we produce the best final seismic image of the subsurface. The tomographically derived velocity model provides velocity information that assists in identifying the geological origin of the imaged reflectors.

For synthetic seismogram modeling we used a program based on the reflectivity method (Fuchs and Müller, 1971), which includes all intralayer multiples and mode conversions as well as absorption. It allows variable structure in the overburden but requires laterally uniform structure in the region where the full waveform is calculated. In our application, this is not a severe restriction because the basalts are locally flat lying and homogeneous. Traveltime tomography, as implemented by Zelt and Smith (1992), is a two-step procedure. Ray tracing through a 2-D velocity model calculates partial derivatives of

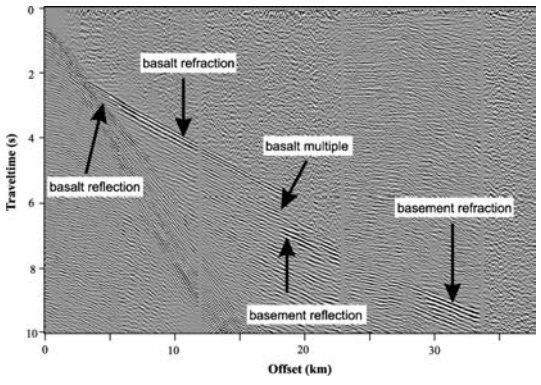

FIG. 2. Example of a supergather from the FLARE profile (see White et al., 1999, for details of how it is constructed from the two-ship data). The main wide-angle phases are labeled. Note the offset of about 1 s between the termination of the basalt refraction and the basement refraction, which is caused by a 3.5-km-thick layer of low-velocity sediments underlying the basalt.

the traveltime with respect to the model parameters (velocity, depth) and the residual traveltimes. The derivatives are then used in an inversion step to update the velocity model. The criteria for stopping the iteration in this procedure are minimal residual traveltimes within the estimated traveltime uncertainty and the ability to trace rays to all observations.

RESULTS

Wide-angle seismic refraction structure

The synthetic supergather shown in Figure 3a was produced from a simple 1-D velocity model (Figure 3b) and includes the full wavefield with all multiples and *P*–*S*-wave conversions. The model incorporates a 1.5-km-thick basalt layer overlying a 3.5-km-thick sedimentary section above basement. The subbasalt sediments have a lower velocity than the layers above and beneath them. The arrivals of interest are the basalt refraction, the wide-angle reflection from the base of the basalt, the reflection from the top of the basement, and the basement refraction.

The time difference between the basalt refraction and the hyperbolic part of the base-basalt reflection is proportional to the thickness of the basalt. With increasing basalt thickness, the base-basalt reflection thus becomes easier to identify as a separate arrival. The term basement is used here to define crust that lies below the rocks of exploration interest, which are the subbasalt sediments. The precritical reflection from the top of the basement is, similar to the base-basalt reflection, often masked by multiple energy and may therefore be difficult to identify, whereas the postcritical reflection is obscured by ringing. The basement refraction is a high-amplitude arrival at far offsets with a greater apparent velocity than the basalt (and the basalt multiple) and is therefore easily identified. The low-velocity sediment beneath the basalt causes a step-back in the first break of about 1 s (Figure 3a). The magnitude of the step-back is controlled by the thickness and the velocity of the low-velocity zone (LVZ), while the offset at which the basalt refraction dies out is controlled by the thickness of the basalt and by the vertical velocity gradient within it.

In real data these arrivals are usually more difficult to observe than on the 1-D synthetic seismogram; in particular, the reflections are often masked by the top-basalt ringing. Figure 4 shows a real-data example, where the basalt refractions and base-basalt reflection are labeled.

Figure 5a shows observed and calculated traveltimes along the line. A regular spacing of 4 km between the observations proved sufficient to constrain the basalt structure. Where the basalt is thinning and eventually dying out (80–40 km), the number of observations was doubled to model the stronger lateral velocity variations in this area. Where the basalt thickness increases to >2 km closer to the Faeroe Islands, it becomes increasingly harder to observe basement arrivals, which are obscured by high-amplitude reverberations from the basalt. The structure beneath the Faeroe Islands themselves is constrained by arrivals recorded by onshore seismometers on the islands (Richardson et al., 1998, 1999).

The velocity model (Figure 5b) was built by working downward layer by layer. For the sedimentary overburden, we used semblance analysis on the 6000-m offset data and a poststack depth-migrated section to define the overburden and top-basalt reflections. Typically, the upper overburden sediment has average velocities around 1.8 km/s, while the deeper sediments immediately above the basalt have velocities of 2.0 to 2.5 km/s, depending on the water depth. The basalt is stratified with an upper 1.5-km-thick layer exhibiting velocities between 4.5 and 5.0 km/s and a lower unit of similar thickness with velocities between 5.0 and 5.5 km/s. The overall velocity gradient is 0.33 s^{-1}. At 30 km, the basalt terminates abruptly (Figure 5b), as documented by the disappearing basalt refraction.

It is always problematic to deduce the velocity of an LVZ because no diving rays are returned from this interval. However,

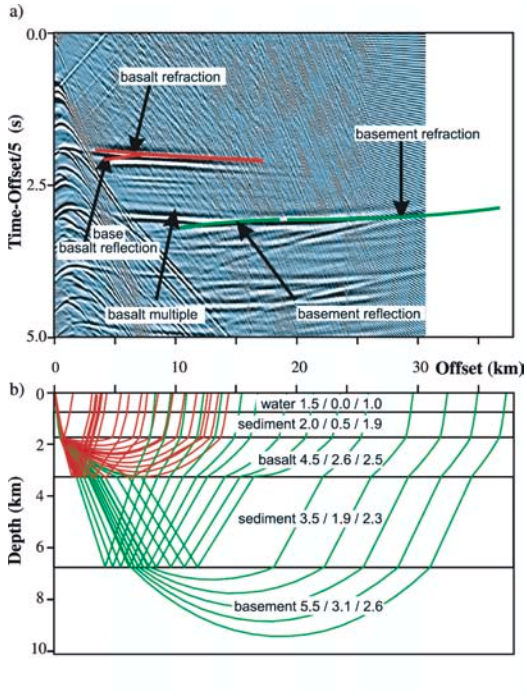

FIG. 3. (a) Full-waveform reflectivity synthetic seismogram model of a single supergather with main phases labeled, using the velocity model shown in (b). Traveltimes reduced at 5 km/s. (b) Example rays traced through the models, with annotated numbers showing *P*-wave velocity (km/s), *S*-wave velocity (km/s), and density (kg/m^3) in each layer.

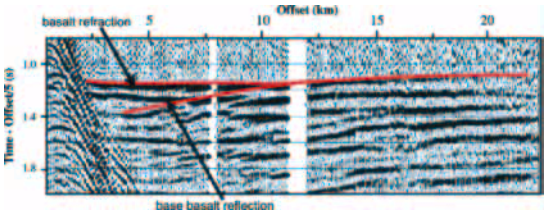

FIG. 4. Enlargement of part of a supergather from the FLARE profile, showing the basement refraction and base-basalt reflections. Traveltimes reduced with 5 km/s.

we are able to constrain these velocities by two methods. First, the move-out of the basement reflections from the base of the LVZ gives information on the average velocity within this interval. Second, the sediments at the same stratigraphic level beyond the feather edge of the basalt flows are not masked by overlying basalt, so their velocities can be found using conventional semblance analysis methods. The subbasalt LVZ has velocities of 3.5–4.5 km/s and an average thickness of about 3 km. Below the LVZ, the basement velocities are only a little higher than those of the basalts and vary along the profile from 5.0 km/s in the southeast to 6.0 km/s in the northwest.

The difficulty of identifying arrivals on real data introduces an uncertainty into the model that is hard to quantify precisely. However, inversion statistics (low chi-squared and residual traveltime values) and perturbation tests performed on individual horizons indicate good agreement between calculated and observed traveltimes within the estimated picking uncertainties of 50 ms for basalt and 100 ms for subbasalt arrivals.

Wide-angle seismic reflection images

The wide-angle wavefield outside the water-wave cone (energy that arrives at large offsets ahead of the sea bottom—white triangle in Figure 6) is most suitable for imaging below the high-velocity basalt because it contains high-amplitude arrivals that have been reflected from the base of the basalt and deeper structures. The first arriving energy beyond the water wave is the basalt refraction, which at greater offsets merges with the base-basalt reflection. At greater offsets, the basement below the basalt becomes the first arrival. Prestack depth migrations of these parts of the data therefore give images that are free from contamination by other arrivals, since they are the first-arriving energy at large offsets. The wide-angle arrivals are also free of many of the interbed multiples and scattered energy that obscure the near-vertical incidence data.

However, the unavoidable disadvantage of using the wide-angle data is that they have a lower frequency content than the near-normal incidence data because the energy has traveled a much longer path. This leads to a lower resolution image of the deep section. Furthermore, when migrating data from large offsets, there is increased danger that inaccuracies in the velocity field will cause the seismic data to be moved to incorrect locations in the final image. Knowledge of the 2-D velocity field and its uncertainty is therefore crucial in constructing and interpreting wide-angle migrations.

Since the move-out of the base- and subbasalt arrivals approaches that of the basalt refraction with increasing offset, the range of move-out velocities in the wide-angle data is small, and constant-velocity stacks of the wide-angle data can also be used to produce a preliminary image—at least for nearly horizontal reflectors. It is important to use a move-out expression that takes account of the nonhyperbolic move-out at far offsets. This procedure can provide a preliminary, qualitative image prior to undertaking the more time-consuming prestack migration. This approach has another advantage in being conservative by not moving energy over far distances and therefore reducing artifacts caused by errors in the velocity field.

First we use the seismic data returned from the base of the basalt and deeper to compare the results of a simple constant-velocity stack (Figure 7a) with a prestack depth migration that uses the full velocity field (Figure 7b). We tested stacks of data from several offset ranges and chose the 6–12-km range as the best overall for the FLARE-1 line. Using data from shorter offsets can make identifying the base-basalt reflector difficult because they contain more internal reflections from the thick basalt sections. Data from considerably larger offsets lack useful signal and resolution. Unfortunately, the 6–12-km offset range suffers from data-acquisition gaps toward the northwestern end of the line (around 160 km), which limits the image quality in that region.

A comparison of the interfaces from the time-converted, ray-traced model with the time-converted constant velocity and prestack depth migrations shows similar results for the

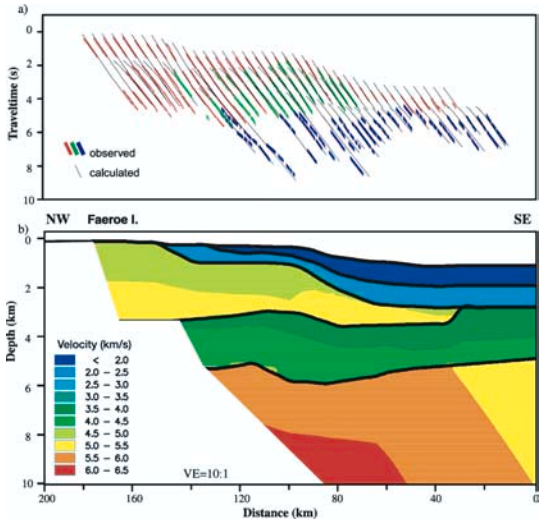

FIG. 5. (a) Calculated traveltimes fit the observed traveltimes within the assumed picking uncertainty of 50 and 100 ms for basalt and subbasalt arrivals, respectively. (b) Velocity model derived from traveltime tomography defines a 3.5-km-thick basalt layer, decreasing in thickness toward the southeast and a nearly 2-km-thick low-velocity layer underneath.

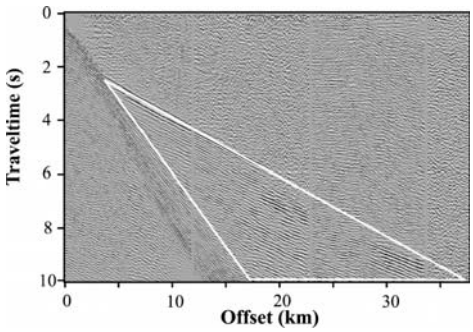

FIG. 6. Example supergather. White triangle outlines the wide-angle arrivals used for migration.

location of the base-basalt reflector on both migrations (overlay lines in Figure 7 are horizons from ray-traced model), although the prestack migration image is stronger (Figure 7b). The constant-velocity stack (Figure 7a) fails to produce an image at the southeastern end of the line, where steeper slopes and a thin basalt provide insufficiently long segments of arrivals for a successful stack. The central part of the profile produces a close match between the onset of wide-angle reflectivity and the ray-traced base-basalt arrival on both sections.

Relatively little seismic energy penetrates the high-velocity basalt and emerges at the surface as subbasalt wide-angle reflections, although amplitudes of such events are expected to be higher than at normal incidence both in absolute values and relative to shallower arrivals. The loss of energy probably is largely because of the inhomogeneous composition of the basalt sequence that includes interfingering thin sediment and tuff layers as well as basalt flows of different thickness, composition, and orientation (Kiørboe and Petersen, 1995). This composition results in substantial energy loss by absorption and scattering. The flat-lying parts of the basalt layer should provide the best opportunities for subbasalt imaging. A prominent arched reflector, partly underlain by a longer northwest-dipping reflector that extends to the southeastern end of the line, appears in the prestack migration at about 50 km and just under 4 s traveltime (Figure 7b). The dipping reflector correlates with the ray-traced basement. Another west-dipping band of reflectivity at 120 km and 2.5 s traveltime is significantly shallower than the basement as interpreted from ray tracing. This could be from a major lithological change within the subbasalt sediments, such as a basaltic sill intrusion. A later, near-parallel event at about 3 s traveltime with lower amplitude is more likely to originate from a block-faulted basement, the details of which could not be resolved by traveltime modeling (the ray-traced model suggests a nearly flat basement at 6 km depth). We chose this central part of the line for a closer examination of the subbasalt image.

The contribution of different offset ranges to the image is illustrated in Figure 8. Although near-offset (200–700 m) data can image structures at all depths, multiple energy completely obscures any primary arrivals below the top of the basalt flows (Figure 8a, processed in the same way as the wide-angle data,

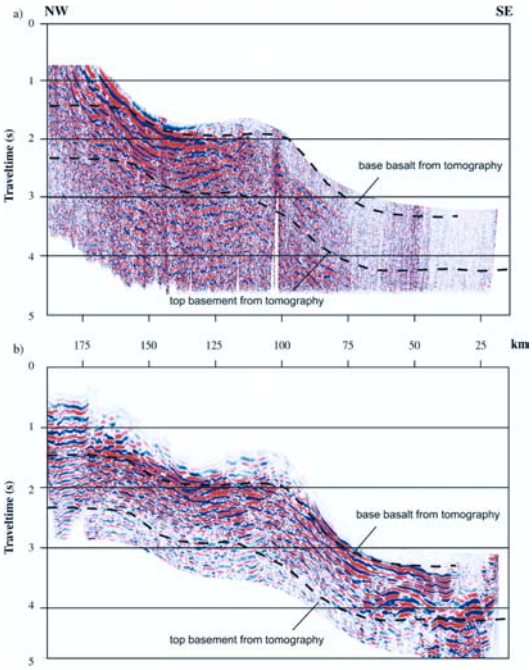

FIG. 7. Comparison of (a) wide-angle, constant-velocity stack (offset range 6–12 km, 4.5 km/s) and (b) prestack depth migration of the same part of the wavefield of the FLARE profile. The depth section was converted to time and muted poststack at the center of the stretched refracted basalt arrival. Locations of the base-basalt and top-basement reflectors, determined from traveltime tomography, are overlain on the profiles.

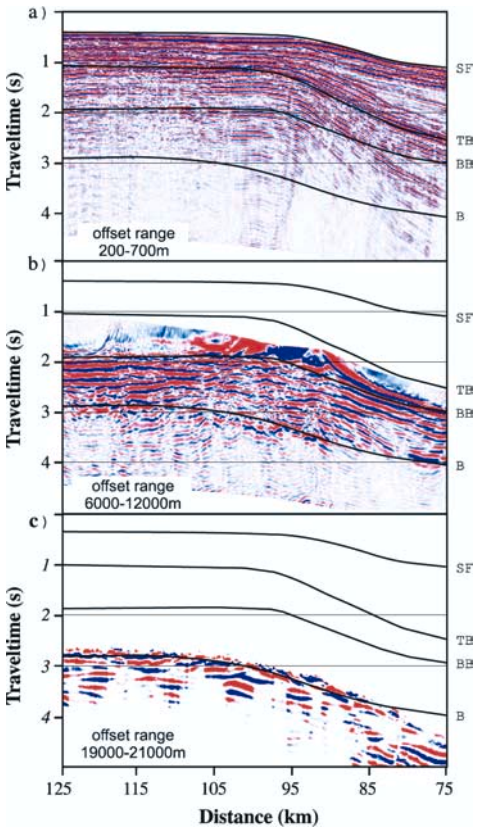

FIG. 8. Prestack depth migration images of the central part of the FLARE profile (line 75–125 km) with contributions from three different offset ranges: (a) normal-incidence offset range; (b) and (c) wide-angle offset ranges excluding data from within the water-wave/top-basalt reflection cone, muted as in Figure 7. Depth axis is converted to time. Principal boundaries of the tomographic velocity model are overlain: SF = seafloor, TB = top basalt, BB = base basalt, B = top basement.

without multiple suppression). The wide-angle images, by contrast, only contain energy from the first-arrival depth and below: the intermediate offsets (6000–12 000 m stack, Figure 8b) from the base of the basalt downwards and the largest offsets (19 000–21 000 m stack, Figure 8c) from the basement. Basement reflection amplitudes are highest at the longer offsets, but the resolution of the image decreases with offset because of the convergence of separate arrivals and the lower frequency content of the data. The intermediate offsets have the potential for a more detailed picture; but the image is dominated by the higher amplitudes of the reflectivity around the base of the basalt flows, which obscures the weaker reflections from the underlying basement. Migrated shot gathers from the central part of the section (Figure 9) show the relative contributions to the stacked image of arrivals from different offsets. Nonprimary reflections and the edges of the data set produce weaker, highly curved arrivals in the migrated gathers; stacking and additional mutes suppress these arrivals where necessary.

At all offsets the basement reflection is clearly separated from the basalt arrivals and is not parallel to the base-basalt arrival at the intermediate and large offset ranges. We can therefore separate out the basement reflection (as done manually for the traveltime tomography) and migrate selectively only that part of the wavefield that contributes to the basement arrivals. Figure 10 demonstrates the effect of this procedure for an intermediate offset range of 12 500–14 000 m. In Figure 10a, the entire wide-angle wavefield between 12 500 and 14 000 m has been migrated, whereas in Figure 10b only a corridor around the basement arrival has been used. The isolated basement image in Figure 10b shows a considerably more rugged basement topography than could have been derived from the coarser sampled traveltime tomography alone. It also demonstrates that the top of the basement is not a single, continuous reflector as has necessarily been assumed for the traveltime analysis.

Near-vertical seismic reflection images

The main problem in near-vertical imaging of the FLARE data is the hard top-basalt interface that produces high-amplitude multiples and the previously mentioned low energy of the subbasalt reflected primaries. The application of an effective multiple suppression technique and subsequent detailed semblance analyses and stacking, however, revealed considerable subbasalt reflectivity, which complements the wide-angle images discussed in the previous section.

Data-consistent deconvolution (Remul/Reson®) was chosen for multiple suppression because of its effectiveness in areas with a hard seabed and in regions with strong lateral velocity variations (Lokhstanov, 1999). This technique models multiple arrivals using the reflectivity pattern of the primary and its periodicity with respect to the intercept time in the τ-p domain. It is therefore able to suppress multiples while preserving primary arrivals of similar move-out. The process is applied for each multiple generating horizon. Figure 11 shows an example of its effectiveness. The main multiples on this gather are from the seabed, from a sedimentary horizon at about 1 s two-way traveltime below the seabed, and from the top of the basalt. Remul/Reson has removed all these multiples successfully and has preserved the top of the basalt and many subbasalt reflections.

Detailed semblance analysis after multiple suppression was performed along the line. Dix conversion to interval velocities is in good agreement with the velocities derived from traveltime tomography in the deepwater part of the line (Figure 12a). Below the shallow waters of the Faeroe shelf, we could not identify any useful semblance and used the tomographic velocity for stacking. The stack obtained from these semblance velocities is shown in Figure 12b. Additional muting of the inner traces was necessary to reduce the amount of residual multiples. Below the shadow produced by the severe inner-trace mute, we observe reflections that are coincident with the migrated wide-angle reflections and the velocity boundary for the base basalt. Toward the deepwater end of the line, the image is more equivocal, showing many reflections of similar character, which make it difficult to identify the base basalt or deeper sedimentary reflections (Figure 13).

DISCUSSION

The results presented above were obtained from different portions of the 38-km offset range and from different basalt and subbasalt arrivals. We used (1) wide-angle refractions and reflections to obtain a tomographic model of the subsurface, (2) wide-angle reflections for prestack depth migration and

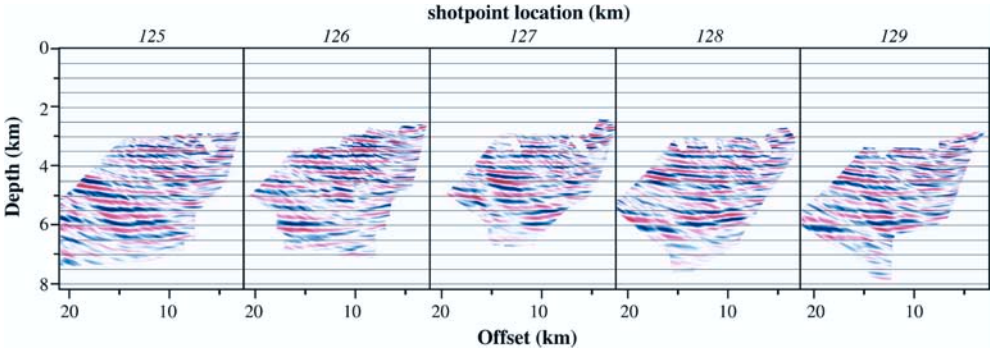

FIG. 9. Depth-migrated shot gathers from the central part of the section showing the entire wide-angle portion of the wavefield. Offsets are trace offsets before migration. Compare shotpoint locations with Figure 7.

constant-velocity stacks, and (3) near-vertical reflections for imaging subbasalt reflectors. Because the results are based on independent observations (different arrivals) from the same target, they should be internally consistent. Wide-angle migration, for example, should not contradict the result from near-vertical migration or tomography. On the contrary, these results should complement and constrain one another to provide a more complete image of the subsurface. Figure 14 illustrates this idea by showing a high-resolution image (from near-vertical migration) for the sedimentary overburden and the basalt and a low-resolution image (from wide-angle migration) for the basalt and the underlying sedimentary section. Additionally, it shows a close match between the results from tomography and near-vertical and wide-angle migration. In the following section, we discuss the contributions to this image and the relative strengths of each of the results. Then we present an interpretation extracted from these components.

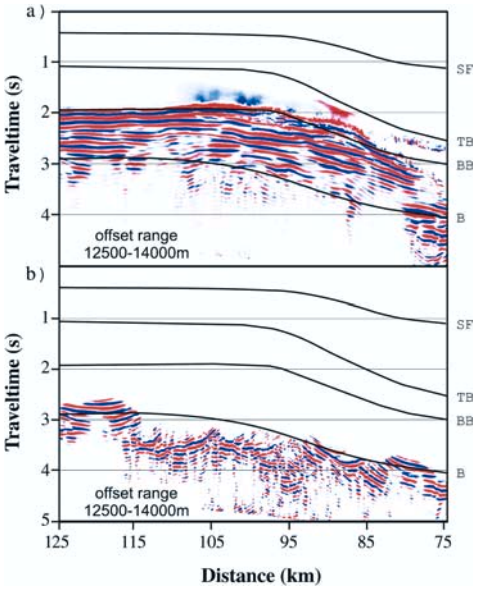

FIG. 10. Comparison of full-wavefield and selective prestack depth migrations of the same offset range. (a) All wide-angle energy in 12.5–14-km offset range (analogous to Figures 8b and c). (b) Energy from top basement reflection only. Depth axis is converted to time. Principal boundaries of the tomographic velocity model are overlain: SF = seafloor, TB = top basalt, BB = base basalt, B = top basement.

Traveltime tomography provides a general (low-resolution) image of the basalt and subbasalt velocities. It is based on refractions and specific wide-angle reflections that constrain the velocity and thickness of the basalt and the low-velocity zone beneath the basalt. The calculated velocity inversion at the base basalt of about 1000 m/s is well beyond the model is uncertainties, which we estimate to be <200 m/s.

The main advantage of using the wide-angle wavefield as outlined in Figure 6 is the lack of energy created above and at the top of the basalt. The basalt diving wave exists as a separate arrival only over a limited offset range before it merges with deeper reflections. Because of the narrow range of move-out velocities for subbasalt arrivals, even a crude and rapid process such as a constant-velocity stack can give a good indication of the shape of the base-basalt reflector. A geometrically correct image can only be achieved by performing migration with the best possible velocity model. Beneath the basalt, this velocity model will only become available after subsequent migration velocity analysis.

The optimal offset range for wide-angle imaging depends on the overburden thickness and the velocity and depth of the target horizons. In our case, the base of the basalt is best observed over offsets between 6 and 12 km; the basement is best observed at offsets >12.5 km. Because of the low-frequency content and hence the low resolution at wide angles, one should only expect to image major structures with high impedance contrasts, such as the base of the basalts and the top of the basement.

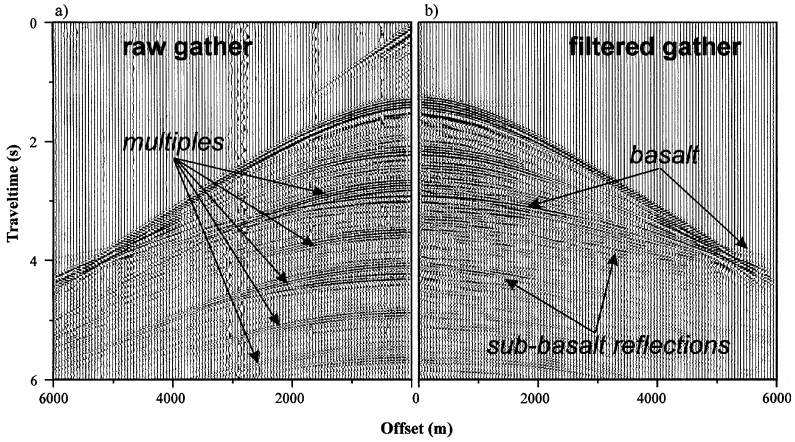

FIG. 11. Shot gather from conventional 0–6 km data on the FLARE profile showing (a) raw data and (b) the same data after removal of multiples using the Remul/Reson algorithm. The direction of increasing offset is swapped in panels (a) and (b) to ease arrival correlation.

The near-vertical arrivals provide the most detailed seismic images but are also the most likely to be misinterpreted because of the residual multiple energy contained in them. Semblance analysis after multiple suppression, however, yields velocities that agree with the results from traveltime tomography, and prestack depth migration with these velocities reveals an interpretable subbasalt reflection. Deeper reflections are present but are too uncertain to be interpreted as intrasediment reflections or as the base of the subbasalt sediments on the basis of this one profile alone.

There is, however, an additional and, from the exploration point of view, valuable piece of information that can be extracted from this image: the termination point of the basalt. The position at which basalt refractions disappear from the supergathers can be used to locate this termination point accurately. In the depth section provided by the near-vertical data set, the location of this termination can be interpreted on the image. Figure 13 shows the thinning basalt and its termination around line 30 km.

Synthesized seismic model

Figure 14 shows our interpretation based on the results presented in this paper. The basalt is thickest beneath the Faeroe Islands and thins gradually toward the center of the Faeroe–Shetland basin, where it eventually terminates. According to Richardson et al. (1999), who recorded the offshore shots from FLARE 96-1 on land, the base of the basalt reaches up to 5 km depth beneath the Faeroe Islands. The basalt is covered by two distinct sedimentary layers that were emplaced from both the Faeroe and Shetland shelves. Beneath the basalt, an approximately 3-km-thick sedimentary layer is present. Strong reflectors within the sedimentary section may be indicative of the presence of basaltic sills. Richardson et al. (1999) found evidence for wedging out the sediment layer toward the Faeroe Islands. The basement probably consists of Lewisian continental crust, apparently with an irregular top probably caused by block faulting during the Mesozoic rifting of the Faeroe–Shetland basin.

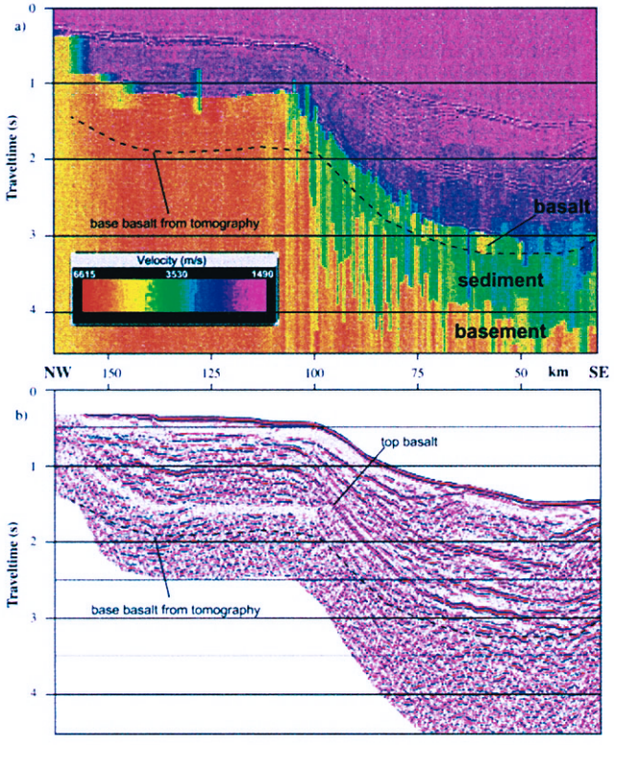

FIG. 12. (a) Detailed semblance analysis after multiple suppression shows a velocity structure similar to the tomographic model. The black line marks the base-basalt boundary from tomography. (b) Controlled stacking (inner and outer trace mutes applied before stacking) reveals a detailed subbasalt image in the deepwater part of the line and some strong and continuous reflections underneath the thicker basalt toward the shelf edge in the northwest.

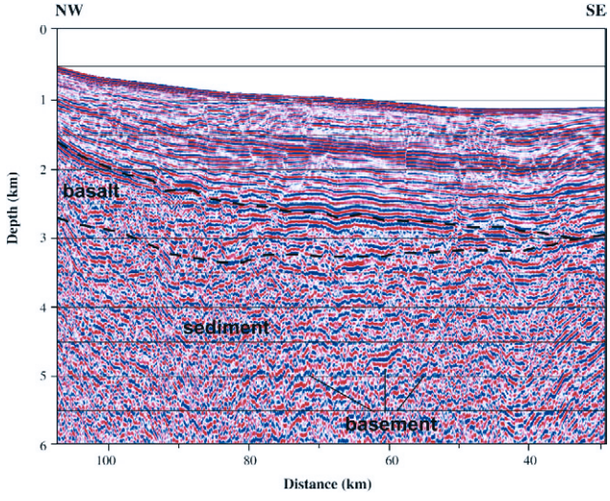

FIG. 13. The *P*-wave prestack depth migration of the near-vertical part of the data set (0–6 km offset), showing termination of the basalt near the southeast end of the profile, disrupted subhorizontal reflections in the subbasalt sediment, and some indication of a top basement horizon.

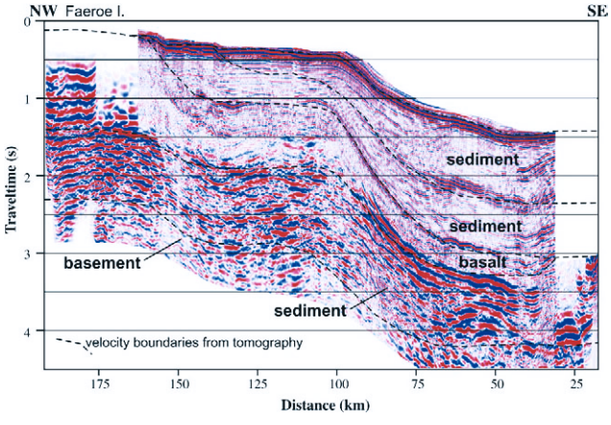

FIG. 14. Synthesized model summarizes the results from all methods and offset ranges. Overburden and basalt layers are constrained by near-vertical data; basalt and subbasalt layers are constrained by wide-angle migration. These results are consistent with the velocity structure derived from wide-angle tomography. Interpretation (basalt/subbasalt) is based on interfaces derived from tomographic inversion.

CONCLUSIONS

Integrating wide-angle and near-vertical techniques is crucial in seismologically difficult areas such as the basalt province of the North Atlantic. The results presented here each use different events of the recorded wavefield, and they constrain and complement one another to provide a more complete image of the subsurface. Traveltime tomography constrains boundaries and velocities of the main layers and proves the existence of subbasalt low-velocity sediments. Wide-angle seismic data provide interpretable horizons that were migrated from middle to far offsets, and conventional seismic reflection data add structural detail to the wide-angle images, such as the thinning and termination of the basalt. The velocities from the wide-angle tomographic inversion enable the reflectors recognized on the best migrated reflection profile to be tagged or identified with their likely origin or rock type. Thus, the prestack depth migration provides the shape of the main interfaces, while the velocity model indicates their probable lithology.

ACKNOWLEDGMENTS

The FLARE-1 profile was conceived by E. Cullen and funded by Western Geophysical and by Amerada Hess and its partners, LASMO, Norsk Hydro, and DOPAS. We thank them all for their support and for permission to publish this article. We are grateful to P. Fontana, W. Kirk, C. Latkiewicz, R. Hardy, and J. R. Smallwood for their advice. We thank Norsk Hydro and particularly Dmitri Lokshtanov, the author of Remul/Reson, for permission and assistance in using their software. J. F. gratefully acknowledges the European Commission for the support of a Marie Curie Fellowship, contract FMBICT961605. M. F. was supported by a grant from Amerada Hess, Dept. Earth Sciences contribution ES 6096.

REFERENCES

Barton, A. J., and White, R. S., 1997a, Crustal structure of the Edoras Bank continental margin and mantle thermal anomalies beneath the North Atlantic: J. Geophys. Res., **102**, 3109–3129.

——— 1997b, Volcanism on the Rockall continental margin: Geol. Soc. London, **154**, 531–536.

Eldholm, O., and Grue, K., 1994, North Atlantic volcanic margins: Dimensions and production rates: J. Geophys. Res., **99**, 2955–2968.

Fuchs, K., and Müller, G., 1971, Computation of synthetic seismograms with the reflectivity method and comparison with observations: Geophys. J. Roy. Astr. Soc., **23**, 417–433.

Kiørboe, L., and Petersen, S. A., 1995, Seismic investigation of the Faeroe basalts and their substratum, *in* Scrutton, R. A., Stoker, M. S., Shimmield, G. B., and Tudhope, A. W., Eds., The tectonics, sedimentation and palaeoceanography of the North Atlantic region: Geol. Soc. London Special Publication **90**, 111–122.

Lokhstanov, D., 1999, Multiple suppression by data-consistent deconvolution: The Leading Edge, **18**, 115–119. See also republication of figures *in* Brown, R. A., 1999, It figures (or does it): The Leading Edge, **18**, 578–585.

Richardson, K. R., Smallwood, J. R., White, R. S., Snyder, D., and Maguire, P. K. H. 1998, Crustal structure beneath the Faroe Islands and the Faroe–Iceland Ridge: Tectonophysics, **300**, 159–180.

Richardson, K. R., White, R. S., England, R. W., and Fruehn, J., 1999, Crustal structure east of the Faroe Islands: Mapping sub-basalt sediments using wide-angle seismic data: Petr. Geosci., **5**, 161–172.

Stoker, M. S., Hitchen, K., and Graham, C. C., 1993, United Kingdom offshore regional report: The geology of the Hebrides and west Shetland shelves and adjacent deep water areas: Her Majesty's Stationery Office.

Waagstein, R., 1988, Structure, composition and age of the Faeroe basalt plateau, *in* Morton, A. C., and Parson, L. M., Eds., Early Tertiary volcanism and the opening of the NE Atlantic: Geol. Soc. London Special Publication **39**, 225–238.

White, R., and McKenzie, D., 1989, Magmatism at rift zones: The generation of volcanic continental margins and flood basalts: J. Geophys. Res., **94**, 7685–7729.

White R. S., Fruehn, J., Richardson, K. R., Cullen, E., Kirk, W., Smallwood, J. R., and Latkiewicz, C., 1999, Faroes large aperture research experiment (FLARE): Imaging through basalts, *in* Fleet, A. J., and Boldy, S. A. R., Eds., Geology of the northwest European continental margin: Geol. Soc. London Special Publication **2**, 1243–1252.

Zelt, C. A., and Smith, R. B., 1992, Seismic traveltime inversion for 2-D crustal velocity structure: Geophys. J. Internat., **108**, 16–34.